IEEE Access
Multidisciplinary | Rapid Review | Open Access Journal

Received January 4, 2019, accepted January 6, 2019, date of publication January 10, 2019, date of current version February 8, 2019.

Digital Object Identifier 10.1109/ACCESS.2019.2891786

Impact of Uncertainties on Resilient Operation of Microgrids: A Data-Driven Approach

AKHTAR HUSSAIN[1], (Student Member, IEEE), ANASTASIOS OULIS ROUSIS[2], (Student Member, IEEE), IOANNIS KONSTANTELOS[2], (Member, IEEE), GORAN STRBAC[2], (Member, IEEE), JINHONG JEON[3], (Member, IEEE), AND HAK-MAN KIM[1], (Senior Member, IEEE)

[1]Department of Electrical Engineering, Incheon National University, Incheon 22012, South Korea
[2]Department of Electrical and Electronics Engineering, Imperial College London, London SW7 2AZ, U.K.
[3]Division of Smart Distribution Research Center, Korea Electrotechnology Research Institute, Changwon 51543, South Korea

Corresponding author: Hak-Man Kim (hmkim@inu.ac.kr)

This work was supported in part by the Korea Institute of Energy Technology Evaluation and Planning, and the Ministry of Trade, Industry, and Energy of the Republic of Korea under Grant 20168530050030, and in part by the Engineering and Physical Sciences Research Council under Grant EP/N034570/1.

ABSTRACT In this paper, the impact of uncertainties in loads, renewable generation, market price signals, and event occurrence time on the feasible islanding and survivability of microgrids is analyzed. A data-driven approach is proposed for estimating the maximum deviation level of uncertain parameters dynamically based on historical data. Similarly, fragility curves are utilized for determining the preparation time for the potential events based on the estimated event occurrence time and physical constraints of the microgrid components. In addition, a resilience-oriented demand response program is proposed for enhancing the utilization of renewables and other available resources for reducing the load shedding during the emergency period. Finally, a resilience index is proposed for quantifying the benefits of the proposed method for the resilience-oriented operation of microgrids. In normal mode, the impact of event occurrence time and uncertainty level is analyzed via an adaptive robust optimization method. In emergency mode, 10 000 Monte Carlo scenarios of all the uncertain parameters are generated, and their impact on the operation cost, amount of load shed, and the range of the proposed resilience index are analyzed for each case.

INDEX TERMS Adaptive robust optimization, demand response, fragility curves, microgrid resilience, uncertainty modeling.

I. INTRODUCTION

A. MOTIVATION

Resilient operation of power systems has recently emerged as a major issue due to the increase of extreme events, e.g. natural disasters and man-made attacks. Extreme events pose severe consequences to power systems in terms of monetary losses, infrastructural damages, and inconvenience to consumers due to extended loss of supply [1]. These events are generally known as low-probability high-impact events due to lower incidences of natural disasters [2]. However, the frequency and intensity of natural disasters, especially extreme weather events, have increased in the last few decades and are expected to increase in the future due to climate change [3]. Seven among the ten major storms of the last four decades have occurred in the last one decade only and each caused damages of over 1 billion dollars. Eight weather-related events have occurred in 2017 only, affecting a minimum of 0.3 million customers in each event [4].

Various studies have been conducted for enhancing the resilience of power systems considering long-term (hardening) and short-term (operational) measures [5]–[13]. This article falls under the latter category; therefore, only operational measures will be discussed in the following paragraphs. Among various potential solutions available in the literature, microgrids are considered as a practical solution for enhancing the resilience of power systems [5]–[13]. This is due to the capability of microgrids to sustain the penetration of distributed energy resources, especially renewables, and the ability of islanding during disruption events [7]. Therefore, numerous studies have focused on utilizing microgrids as a resilience resource for surviving critical loads. However, the performance of the microgrids is influenced by both

prevailing and event-related uncertainties. Uncertainties in loads, renewables, and market price signals are termed as prevailing uncertainties. Similarly, uncertainties associated with event occurrence time and event clearance time are known as event-related uncertainties.

B. RELATED WORK

The existing literature on enhancing the resilience of microgrids can be divided into two major categories, i.e. microgrids as a resilience resource and strategies used by microgrids for enhancing their resilience. This article falls under the latter category. The following two sub-sections summarize the existing literature on both of the categories.

1) MICROGRIDS AS A RESILIENCE RESOURCE

Various studies are available in the literature for using microgrids as a resilience resource during major outages [6]–[13]. Microgrids are used for restoration of critical loads of distribution system by prioritizing loads in [6] and [7]. A strategy table having all feasible restoration paths is developed by [6] and coverage maximization of critical loads is considered by [7]. In order to enhance the resilience of distribution networks, formation of microgrids is suggested by [8] and [9]. The on-outage area is sectionalized into self-adequate microgrids by [8] and dynamic microgrids formation after events is considered by [9]. The optimal placement of distributed generators for formulation of self-adequate microgrids during major events is studied in [10]. The dynamic formation of microgrids after major events can be computationally demanding due to the introduction of various new variables. Therefore, a study is conducted in [11] for reducing the computational time for the formation of microgrids. Due to the absence of universally accepted resilience indices, four indices are proposed in [12] for analyzing the resilient performance of power systems in extreme conditions. Schneider *et al.* [13] have analyzed the use of microgrids as a local resource, a community resource, and a black-start resource.

It can be observed from the previous discussion that plenty of literature is available for using microgrids as a resilience resource. However, in order to use the microgrids as a resilience resource, they need to be prepared for these events, i.e. resilience-oriented operation of microgrids is required. In this paper, resilience is defined as the ability of a microgrid to prepare for an upcoming potential event and withstand the event by feeding at least its most critical loads during the event period. Strategies used by microgrids for enhancing their resilience is also gaining popularity, which is discussed in the following sub-section.

2) STRATEGIES USED BY MICROGRIDS FOR ENHANCING THEIR RESILIENCE

Recently, some studies have been focusing on strategies used by microgrids for enhancing their resilience [14]–[19]. Proactive scheduling of microgrids is proposed by [14] and [15] for the pre-event phase. In [14], the vulnerable components are identified first and then the outage of all vulnerable component is considered during extreme floods. In [15], the objective is to minimize the damage caused by islanding events via pre-event preparedness. Similarly, a post-event survivability enhancement mechanism is proposed in [16], where extended outage duration of events is considered and optimal utilization of storage elements is proposed. Resiliency-oriented operation schemes for both grid-connected and islanded modes of microgrids are proposed in [17]–[19]. Dynamic penalty cost and the next day operation are considered in [17] to enhance the survivability of critical loads. Resiliency cuts are introduced to revise the schedule of microgrid components in [18] for feasible islanding. Similarly, physical constraints of microgrid components are considered in [19] while updating scheduling windows during emergencies.

C. RESEARCH GAPS AND CONTRIBUTIONS

1) RESEARCH GAPS IN THE EXISTING LITERATURE

Most of the resilience-oriented operation studies have assumed that the event occurrence time is known in advance [14]–[19]. However, prediction of exact event occurrence time is difficult for resilience related events. This assumption might result in inappropriate scheduling of microgrids for upcoming events. Instead, the event occurrence time can be estimated using fragility curves, especially for weather-related events. In case of weather-related events, initial warnings are issued from the metrological agencies. The information of the particular parameters (seismic activities for earthquakes, wind speed for wind storms, direction and speed of clouds for heavy rains, direction and speed of water for floods, etc.) can be utilized to estimate the readiness time for a microgrid.

The formulations in [17] and [18] are based on robust optimization with fixed uncertainty bounds and a deterministic formulation is considered in [19]. The fixed uncertainty bounds are not capable of capturing dynamics across different times of the day, days of the week, and seasons of the year, thus resulting in under or over-estimation of uncertainties. This might result in failure to achieve the set resilience target during outages. Additionally, resilience-oriented demand response (DR) programs were not considered in any of these studies [14]–[19]. However, time insensitive non-critical loads can be shifted across different time intervals to reduce load shedding and to better utilize renewables.

2) PROPOSED METHOD AND MAJOR CONTRIBUTIONS

In order to address the challenges and to achieve the potential benefits mentioned in the previous paragraphs, a data-driven approach is proposed to estimate dynamic uncertainty bounds in this study. Historical data are utilized to estimate the dynamic uncertainty bounds for each interval. The dynamic uncertainty bounds are capable of capturing dynamics across different days of the week and different hours of the day. Event data are utilized to build fragility curves for determining readiness time. The readiness time (time for

activation of the resilience-oriented scheduling) can be decided based on the pre-heat/startup time of CDGs and C-rates of energy storage elements of the microgrid. Additionally, a DR program is proposed to enhance the service reliability of loads during the emergency period by adjusting them. The proposed DR program can reduce the curtailment of renewables on one hand and can reduce the shedding of loads on the other hand. Reduction of renewable curtailment results in higher benefit for the renewable owners and reduction in load shedding enhances the comfort level and reduces the monitory loss of the consumers. Finally, an adaptive robust optimization method is employed to analyze the performance of the proposed method in the normal operation phase. Operation cost, load shedding amount, and the proposed resilience index are analyzed by using ten thousand Monte Carlo simulation scenarios, in the emergency phase. The major contributions of this article in comparison with the existing literature are as follows.

- A data-driven dynamic uncertainty bound estimation method is proposed in this study, in contrast to [14]–[19], where either static uncertainty bounds are considered or deterministic approaches are utilized. The proposed method has the capability to capture dynamics across different hours of the day and different days of the week.
- In contrast to [14]–[19], where known event time is assumed, fragility curves are utilized for deciding the readiness time during the proactive operation phase. Physical constraints of microgrid components are considered for deciding the activation time of the proactive operation algorithm.
- A DR program is proposed for the emergency phase to enhance the resiliency of the system by adjusting load profiles, which was not considered in [14]–[19]. The proposed DR method can benefit both renewable owners and microgrids consumers by reducing renewable curtailment and load shedding amount.
- Realistic assumptions for major events, i.e. limited supply of fuel, persistence of event in the following days along with real data of load, market price, and renewables are considered. These considerations are ignored in whole or in part in the existing studies.

II. SYSTEM CONFIGURATION AND PROPOSED UNCERTAINTY MODELING

A. SYSTEM CONFIGURATION

The configuration of the hybrid AC/DC microgrid considered in this study is shown in Fig. 1. Both AC and DC microgrids contain controllable distributed generators (CDGs), renewable distributed generators (RDGs), battery energy storage systems (BESSs), and critical and non-critical loads. The AC microgrid is connected to the utility grid, while the DC microgrid contains electric vehicles (EVs). Both microgrids can exchange power via the interlinking converter. The proposed DR program can be activated by both the microgrid sides.

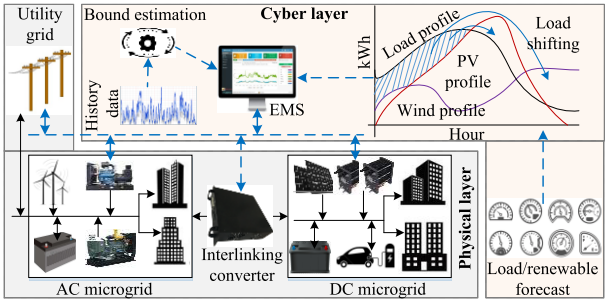

FIGURE 1. Overview of the proposed hybrid microgrid network.

The energy management system (EMS) is responsible for the optimal operation of the hybrid microgrid in both grid-connected and islanded modes with respective objectives and constraints. The EMS also estimates the bounds for uncertainty deviations of the uncertain parameters. Similarly, the DR program, which uses the forecasted information of loads and renewables, is also incorporated into the EMS. All the components of the microgrid follow the EMS commands.

B. PROPOSED DATA-DRIVEN UNCERTAINTY MODELING

1) LOADS, RENEWABLES, AND MARKET PRICE

The loads, renewables, and market prices are subject to variations. Therefore, the uncertainties in these three parameters can be modeled as a polyhedral set, as in equation (1), to maintain the linear tractability of the model [20]. Where Υ_t represents the deviation level of the uncertain parameter at interval t. Equation (1) can be represented as a simplex by (2)-(5) to keep the model linear. Where Ψ represents the uncertain parameter and Γ_Ψ represents the budget of uncertainty for that parameter. The budget of uncertainty corresponds to the number of intervals during which the uncertain parameter Ψ can deviate from the forecasted values. It controls the conservatism of the solution and it can be decided using historical data or based on the experience of the operators. Generally, worst-case scenario (allowing the uncertain parameter to deviate in all the intervals) is considered and instead maximum deviation level for each interval is controlled. $\overrightarrow{P}_{\Psi,t}$, $\overleftarrow{P}_{\Psi,t}$, and $\Delta P^{max}_{\Psi,t}$ respectively represent an upper bound, lower bound, and maximum uncertainty deviation for the uncertain parameter Ψ. Uncertainty deviation corresponds to the value of mismatch between the actual and the corresponding forecasted value of the uncertain parameter Ψ.

Equation (2) shows that the uncertainty deviation level can be computed using upper and lower bounds of uncertainty deviation. However, any uncertain parameter can either take the upper or lower bound only for a particular interval, not both. Both upper and lower bounds can take a maximum value of $\Delta P^{max}_{\Psi,t}$, as given by Equation (3). Equation (4) shows that the total number of intervals deviating from their forecasted values, during the entire scheduling horizon, need to be lesser than or equal to the budget of uncertainty. Finally, the actual amount ($P_{\Psi,t}$) of an uncertain parameter can be determined

using its forecasted value ($P^{*}_{\Psi,t}$) and uncertainty deviation level ($\Delta P_{\Psi,t}$), as given by (5).

$$U = \left\{ \Upsilon \,|\, |\Upsilon_t| \le \Upsilon_t^{max} \wedge \sum_{t \in T} |\Upsilon_t| \Big/ \Upsilon_t^{max} \le \Gamma \;\forall t \in T \right\} \tag{1}$$

$$\Delta P_{\Psi,t} = \vec{P}_{\Psi,t} - \underrightarrow{P}_{\Psi,t} \quad \forall t \in T \tag{2}$$

$$\vec{P}_{\Psi,t} \le \Delta P_{\Psi,t}^{max}, \quad \underrightarrow{P}_{\Psi,t} \le \Delta P_{\Psi,t}^{max} \;\forall t \in T \tag{3}$$

$$\sum_{t \in T} \left(\vec{P}_{\Psi,t} + \underrightarrow{P}_{\Psi,t} \Big/ \Delta P_{\Psi,t}^{max} \right) \le \Gamma_{\Psi} \tag{4}$$

$$P_{\Psi,t} = P^{*}_{\Psi,t} \left(1 - \Delta P_{\Psi,t}\right) \quad \forall t \in T \tag{5}$$

The maximum deviation level ($\Delta P_{\Psi,t}^{max}$) in this model is an important decision parameter and it controls the deviation level of uncertain parameters from the forecasted values. Generally, a symmetrical [17] or a non-symmetrical [14], [15] but fixed ratio of the forecasted value is added/subtracted and taken as the maximum deviation level. However, the uncertain parameters do not follow a fixed pattern throughout the day and thus the uncertainty is miscalculated via the fixed ratio. In order to address this problem, a data-driven dynamic ratio is estimated using historical data for each interval of the operation day in this study. Algorithm 1 shows the estimation procedure of the proposed data-driven dynamic ratio. The data of an uncertain parameter at each interval are initially divided into n bin edges and the corresponding probabilities are computed using historical data. Forecasted values for each interval are taken as the starting point and a target value of probability (confidence level in %) are taken as inputs. Starting with the forecasted values, the required confidence level is achieved by searching across the bin edge data. The confidence level can be set to 100% for fully robust operation. However, it results in over-conservative solutions by considering the worst-case during all the intervals. Due to the utilization of dynamic ratio, better robustness can be achieved owing to day/interval-specific consumption/generation analysis even at lower confidence levels. Then, the maximum deviation of the uncertain parameter is determined using the upper and lower bounds corresponding to the defined confidence level. The upper and lower bounds are determined using the bin edge data of corresponding upper and lower levels within the specified confidence level. The selection of upper/lower bound depends on the nature of the uncertain parameter, i.e. an upper bound will be selected for load and a lower bound for renewables. Finally, by using the selected upper/lower bound and the forecasted value of the parameter Ψ, the maximum deviation level for interval t is determined, as shown in line 18 of Algorithm 1.

Algorithm 1: Determining Maximum Deviation of Uncertain Parameters

1 Get bin edge data and corresponding probability for each range
2 Determine normalized probability ($NProb_t$) for each range
3 Get forecasted values of uncertain parameters for each interval (t)
4 **for all** $t \in T$ **do**
5 Determine the range index (I_t) and the corresponding probability ($NetProb_t$) of forecasted data. Define acceptable value (χ_t)
6 Append -1 at the beginning and end of $NProb_t$
7 Initialize: c1, c2=1; upper index, lower index ($UI_t, LI_t = I_t + 1$)
8 **While** $round(NetProb_t) < \chi_t$ **do**
9 **If** $NProb_{I_t+k1} \ge NProb_{I_t-k2}$ **then**
10 Update net probability: $NetProb_t += NProb_{I_t+k1}$
11 Update: $UI_t = I_t + k1, k1++$
12 **else**
13 Update net probability: $NetProb_t += NProb_{I_t-k2}$
14 Update: $LI_t = I_t - k2 - 1, k2++$
15 **end if**
16 **end while**
17 Determine upper and lower bounds (UB_t, LB_t) using bin edge data
18 Determine maximum deviation of the uncertain parameter: $\Delta P_{\Psi,t}^{max} = \left| (P^{*}_{\Psi,t} - B) \Big/ P^{*}_{\Psi,t} \right|, B = \max\{UB_t, LB_t\} \perp \min\{UB_t, LB_t\}$
19 **end for**

2) EVENT UNCERTAINTY AND READINESS MODELING

Resilience-oriented scheduling of microgrids is challenging due to unknown event time. Where event time is the time at which a particular natural disaster hits the under consideration microgrid. However, in the case of extreme weather-related events (the major cause of large-scale power outages), initial warnings from the local meteorological agencies are issued. The information related to particular events, i.e. seismic activities for earthquakes, wind speed for wind storms, direction and speed of clouds for heavy rains, direction and speed of water for floods, etc. can also be monitored. Similarly, the vulnerability of a particular line or a tower can also be estimated based on the history of events in the same or similar localities. Therefore, this information can be utilized to improve the economic and resilience performance of the microgrids.

Conventional resilience-oriented scheduling of microgrids results in conservative solutions, which are not economically efficient. Therefore, this type of scheduling cannot be carried out throughout the year. Event occurrence information is required to decide the starting point of the resilience-oriented scheduling. The point at which the probability of collapsing the under consideration line is above a particular threshold is considered as the event occurrence time. This point can be determined by using the wind speed and direction information along with the wind propagation profile, i.e. increasing or decreasing. This information is conveyed to the

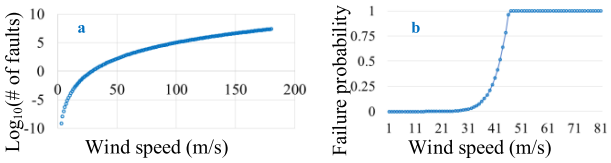

FIGURE 2. No. of overhead lines faults and failure probability vs wind speed.

EMS to activate the proactive operation considering its local components. The resilience-oriented scheduling time can be decided based on the pre-heat/startup time of CDGs and C-rates of energy storage elements of the microgrid. The slowest component in terms of time to achieve the required resilience level is considered as the bottleneck of the system. Therefore, the proactive operation is activated considering the capability of the slowest component, to assure the required resilience to the critical loads.

However, accurate estimation of event occurrence time is challenging [21]. Therefore, in this paper, a fragility curve model is adopted to link the event occurrence probability to weather-related events. Due to the significant impact of windstorms on the power system, the method for utilizing wind speed information to estimate the islanding of microgrids is presented in this section. However, this type of fragility curves analysis can be utilized for most of the extreme-weather related events, i.e. windstorms, ice storms, floods, typhoons, earthquakes, and heavy rains. The particular parameter(s) for each event can be analyzed against the failure of distribution lines. It has been reported in [22] that from all weather-related events, windstorms have caused the largest number of faults in the UK's power systems. Therefore, in this paper, a fragility curve has been constructed that shows the failure probability of overhead distribution lines as a function of wind speed. The actual number of failures of overhead lines in the UK's distribution network when subjected to windstorm hazard, as reported within the National Fault and Interruption Report Scheme database [23], are shown in Fig. 2a. Where the fault/failure of a line refers to the outage of the line due to higher wind speed. In this study, fault/failure of a line is synonymous to line collapse due to extreme weather conditions, i.e. wind speed in this example. Log data are plotted to visualize the lower wind speed impact also, where negative values correspond to less than one fault. Same data are utilized to develop the fragility curve of Fig. 2b using (6) [23], [24]. Where, $Pr(v)$ is the probability of line failure at wind speed v, $v_{collapse}$ is the wind speed at which the line will collapse, F_{pkm} is the number of faults per km, and L_{pa} is the average length of overhead lines between two poles.

$$Pr(v) = \begin{cases} 1 & if\ v \geq v_{collapse} \\ F_{pkm}/L_{pa} & else \end{cases} \quad (6)$$

3) RESILIENCE-ORIENTED DEMAND RESPONSE

Demand response can benefit both the utilities and the consumers by controlling the load profiles instead of generation. DR programs are generally triggered by market price signals to reduce the peak load demand in grid-connected microgrids. Several studies are available in the literature on the use of price-based and incentive-based DR programs for grid-tied microgrids [25]–[27]. Similarly, studies on utilizing DR programs for voltage and frequency regulation of islanded microgrids are also available in the literature [28]–[30]. These researches either utilize incentive-based DR (incentivizing customers to reduce load during low generation intervals) or energy storage elements (to store the excess of renewable power). Due to limited capacity of storage elements, renewables are curtailed during peak generation intervals, while load shedding is employed at peak load intervals. This reduces the benefit to renewable generation owners and causes discomfort to the customers. Resilience-oriented DR programs for shifting non-critical and time insensitive loads across different intervals of the scheduling horizon are not considered in these studies.

Therefore, a resilience-oriented DR program is proposed in this paper to enhance the resilience of shiftable, non-critical loads during the emergency period. This program enhances the service reliability to consumers on one hand and increases the utilization of renewables on the other hand. During off-peak load intervals, the available CDGs may not be fully utilized, while loads may be curtailed during peak load intervals due to insufficient storage capacity. This problem can also be mitigated by using the proposed DR program via shifting loads from peak intervals to non-peak intervals. The mathematical model of the proposed DR program is shown in the next section.

III. PROBLEM FORMULATION: NORMAL MODE

The normal mode base model (deterministic model) considered in this study is same with that of [19]. The base model contains the constraints for CDGs, power balancing, BESS, EVs, readiness, and interlinking converter. CDG constraints include maximum/minimum generation bounds along with startup and shutdown cost constraints. Power balancing constraints are comprised of AC and DC side power balancing equality constraints. BESS and EV constraints comprise of charging/discharging, state-of-charge (SOC), and charging/discharging efficiency constraints. EV contains additional constraints also for target SOC before its departure time. Finally, interlinking converter constraints comprise of capacity and efficiency constraints. Detailed models can be seen in [19].

Robust optimization has gained popularity due to its inherent merits over other uncertainty handling techniques, as mentioned in [31] and [32]. The standard robust optimization is a static optimization method, where the uncertainties of the entire scheduling horizon are revealed together. In order to address this shortcoming, a two-step dynamic adaptive robust optimization method is proposed by [33]. Where, the continues variables are adjusted according to the revealed values of uncertainties. Due to this merit, adaptive robust optimization is utilized in this study. In adaptive robust

optimization, initially, a deterministic model is formulated, which is as follows.

A. DETERMINISTIC MODEL

The compact form of the deterministic model for grid-connected mode is shown in equations (7)-(9). In (7), $\mathbf{x}$ is the vector of binary variables (day-ahead decision variables) and $\mathbf{y}$ is the vector of continuous variables (uncertainty-related variables). In (8), $\mathbf{Ax} \leq \mathbf{b}$ represents the constraints related to day-ahead decisions of CDGs, i.e. start-up, shut-down, and running cost constraints. In (9), $\mathbf{Fy} \leq \mathbf{g}$ represents the constraints for continuous variables, i.e. power balance, BESS, EV, power trading with the grid, and power transfer among AC and DC microgrids. $\mathbf{Gy} \leq \mathbf{r} - \mathbf{Px}$ represents the constraints for generation limits and ramp rates of CDGs. $\mathbf{Ry} \leq \mathbf{h}$ represents the resiliency constraints for feasible islanding. Finally, $\mathbf{Uy} = \Psi^{lr}$ and $\mathbf{Ey} = \Psi^{p}$ represent the uncertainty constraints for loads/ renewables and market prices, as defined in (2)-(5).

$$\min \mathbf{c}^{\mathrm{T}}\mathbf{x} + \mathbf{d}^{\mathrm{T}}\mathbf{y}(\mathbf{x}, \Psi^{lr}, \Psi^{p}) \tag{7}$$

$$\text{Subject to : } \mathbf{Ax} \leq \mathbf{b}, \mathbf{x} \in \{0, 1\} \tag{8}$$

$$\Omega(\mathbf{x}, \Psi^{lr}, \Psi^{p}) = \begin{Bmatrix} \mathbf{Fy} \leq \mathbf{g}, & \mathbf{Gy} \leq \mathbf{r} - \mathbf{Px}, \mathbf{Ry} \leq \mathbf{h}, \\ \mathbf{Uy} = \Psi^{lr}, & \mathbf{Ey} = \Psi^{p} \end{Bmatrix} \tag{9}$$

B. ADAPTIVE ROBUST COUNTERPART

The deterministic model of (7)-(9) can be decomposed into binary and continuous parts and can be re-written as following.

$$\min \mathbf{c}^{\mathrm{T}}\mathbf{x} + \max_{\Psi^{lr}, \Psi^{p} \in U} \min_{\mathbf{y} \in \boldsymbol{\Omega}(\boldsymbol{x}, \Psi^{lr}, \Psi^{p})} \mathbf{d}^{\mathrm{T}}\mathbf{y}(\mathbf{x}, \Psi^{lr}, \Psi^{p})$$
$$\text{Subject to : (8), (9).} \tag{10}$$

The two-stage problem of (10) is hard to solve due to the min-max-min nature. Therefore, a two-level algorithm is adopted to efficiently solve the problem. The problem is decomposed into inner and outer level sub-problems, which are discussed in the following sub-sections.

1) INNER LEVEL SUB-PROBLEM

The max-min part of (10) along with (9) is named as the inner problem. The inner problem is hard to solve in this form due to the max-min nature of the problem. The inner problem can be transformed into a maximization problem by taking its dual, as given by (11)-(13). Where, $\boldsymbol{\lambda}$, $\boldsymbol{\pi}$, $\boldsymbol{\mu}$, $\boldsymbol{\varphi}$, and $\boldsymbol{\nu}$ are the dual variable vectors introduced for the duality of the inner problem. U is the set of uncertainty constraints defined in (1). The second term of the dual objective function has bilinear terms, which can be linearized by following the method suggested in [34].

$$\max_{\Psi^{lr}, \Psi^{p}, \boldsymbol{\lambda}, \boldsymbol{\pi}, \boldsymbol{\nu}, \boldsymbol{\varphi}} -\boldsymbol{\lambda}^{\mathrm{T}}\mathbf{g} - \boldsymbol{\pi}^{\mathrm{T}}(\mathbf{r} - \mathbf{Px}) - \boldsymbol{\mu}^{\mathrm{T}}\mathbf{h} + \boldsymbol{\nu}^{\mathrm{T}}\Psi^{lr} + \boldsymbol{\varphi}^{\mathrm{T}}\Psi^{p} \tag{11}$$

$$\text{Subject to : } -\boldsymbol{\lambda}^{\mathrm{T}}\mathbf{F} - \pi^{\mathrm{T}}\mathbf{G} - \boldsymbol{\mu}^{\mathrm{T}}\mathbf{R} + \boldsymbol{\nu}^{\mathrm{T}}\mathbf{U} + \boldsymbol{\varphi}^{T}\mathbf{E} = \mathbf{d}^{\mathrm{T}} \tag{12}$$

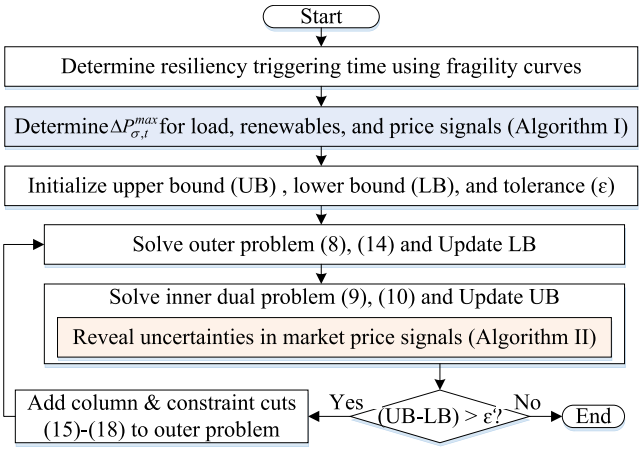

FIGURE 3. Solution method for adaptive robust optimization.

$$\boldsymbol{\lambda} \geq 0, \quad \boldsymbol{\pi} \geq 0, \ \boldsymbol{\mu} \geq 0, \ \boldsymbol{\varphi},$$
$$\boldsymbol{\nu} \text{ free(both + and -)}, \quad \Psi^{lr}, \ \Psi^{p} \in U \tag{13}$$

2) OUTER LEVEL SUB-PROBLEM

The binary decision part of (10) combined with (8) is named as the outer problem. The outer problem is subjected to additional constraints (15)-(18), known as column & constraints cuts. If both the inner and outer problems do not converge, a set of new cuts, as defined in (15)-(18), are added after each iteration. The objective of these cuts is to reduce the convergence time. The column & constraints cuts, being primal plane cuts, are more efficient than Bender's decomposition [34], which are dual plane cuts.

$$\min_{\mathbf{x}, \vartheta, \mathbf{y^k}} \mathbf{c}^{\mathbf{T}}\mathbf{x} + \vartheta \tag{14}$$

Subject to: (8) and the following constraints

$$\vartheta \geq \mathbf{d}^{\mathbf{T}}\mathbf{y}^{k}, \quad k = 1, 2, 3...., K \tag{15}$$

$$\mathbf{Fy}^{k} \leq \mathbf{g}, \quad k = 1, 2, 3...., K \tag{16}$$

$$\mathbf{Gy}^{k} \leq \mathbf{r} - \mathbf{Px}, \quad k = 1, 2, 3...., K \tag{17}$$

$$\mathbf{Ry}^{k} \leq \mathbf{h}, \quad k = 1, 2, 3...., K \tag{18}$$

C. SOLUTION METHOD

The inner and dual of the outer problems are iteratively solved to achieve the optimal results, as shown in Fig. 3. After estimating the event occurrence time and maximum deviation level of uncertain parameters, the outer problem is solved. Then the worst-case uncertainties in market price are determined using Algorithm 2. Finally, the inner problem is solved and convergence is assessed. Where ε represents the tolerance for the mismatch between the upper and the lower bounds. Generally, a minute value is assigned to ε to assess the convergence of the solution. The column & constraints cuts are added after each iteration to expedite the problem's convergence speed.

Algorithm 2: Determining Worst-Case Market Price Signals

Get forecasted values of market price signals Get $\Delta P^{max}_{\sigma,t}$ from Algorithm 1 and Γ_σ
Sort the forecasted values in descending order ($SP^*_{\sigma,t}$) and maintain the original index in an array (OI_t)
for all $t \in T$ **do**
  If $t \leq \Gamma_\sigma$ **then**
    Determine worst-case price: $WP_{\sigma,t} = SP^*_{\sigma,t}(1 \pm \Delta P^{max}_{\sigma,t})$
  else
    Determine worst-case price: $WP_{\sigma,t} = SP^*_{\sigma,t}$
  end if
end for
for all $t \in T$ **do**
  Determine the revealed values of price signals ($P_{\sigma,t}$) $P_{\sigma,t} = SP^*_{\sigma,In}$; *where*, $In = OI_t$
end for

IV. PROBLEM FORMULATION: EMERGENCY MODE

The base problem of the emergency mode operation (islanded mode) is similar to that of the grid-connected mode operation, except few changes. Instead of power trading with the utility grid, load shedding of critical and non-critical loads is considered in the emergency mode. Similarly, instead of readiness constraints, survivability constraints are considered in the emergency mode. Survivability constraints include precedence between charging of the battery for later usage and feeding of non- critical loads. Finally, resilience-oriented demand response constraints are included in the emergency mode operation.

A. OBJECTIVE FUNCTION AND CONSTRAINTS

The objective function of the islanded mode is given by (19) where, **x** represents binary decision variables, while **y** and **z** represent continuous variables. **z** is introduced in the islanded mode to capture variables related to load shedding and DR. In (19), **p** represents the penalty cost for shedding loads and **v** represents the penalty cost for shifting loads, as defined in (24). Similar to grid-connected mode, (20) represents the constraints related to the start-up, shutdown, and running cost of CDGs. In (21), $\mathbf{Fy} \leq \mathbf{g}$ represents the constraints for power balance, BESS, EV, and power transfer among AC and DC microgrids. The power balance in islanded mode is different from grid-connected mode due to the absence of the connection with the grid and introduction of DR. Power buying is replaced with load shedding and an adjusted load (25) is used instead of the original load. In (21), $\mathbf{Gy} \leq \mathbf{r} - \mathbf{Px}$ represents the constraints for generation limits and ramp rates of CDGs. $\mathbf{Cz} \leq \mathbf{h}$ represents the penalty cost constraints for the shedding of critical loads, non-critical loads, and other survivability constraints for switching of the scheduling horizon. Penalty cost of non-critical loads should be less than that of critical loads and greater than the most expansive CDG's generation cost. This relationship will assure the precedence of service reliability over cost in the islanded mode. Finally, $\mathbf{Dz} \leq \mathbf{d}$ represents the DR constraints for non-critical loads, as defined in (22)-(24).

$$\min \mathbf{c}^{\mathrm{T}}\mathbf{x} + \mathbf{d}^{\mathrm{T}}\mathbf{y}(\mathbf{x}, \Psi_s^{lr}, \Psi_s^{p}) + (\mathbf{p}^{\mathrm{T}} + \mathbf{v}^{\mathrm{T}})\mathbf{z}(\Psi_s^{p} + \Psi_s^{lr}) \quad (19)$$

$$\text{Subject to : } \mathbf{Ax} \leq \mathbf{b}, \quad \mathbf{x} \in \{0, 1\} \quad (20)$$

$$\Omega(\mathbf{x}, \Psi_s^{lr}, \Psi_s^{p}) = \left\{ \begin{matrix} \mathbf{Fy} \leq \mathbf{g}, \mathbf{Gy} \leq \mathbf{r} - \mathbf{Px}, \\ \mathbf{Cz} \leq \mathbf{h}, \mathbf{Dz} \leq \mathbf{d} \end{matrix} \right\} \quad (21)$$

B. DEMAND RESPONSE CONSTRAINTS

Amount of load to be shifted from time intervals t′ to t ($P^{ls}_{t',t}$) can be computed using (22). In order to avoid inconvenience, shifting is not allowed to those intervals having load shedding (P^{nl}_t) already. The load shifting from t′ to t is limited by the amount of shiftable load present at this interval (P^{Shift}_t), as given by (23). $TO^{\max}_t$ and $FR^{\max}_t$ are the maximum amount of inflow and outflow capacity of interval t. Equation (24) shows that a huge penalty ($v_{t,t'}$) is imposed if shifting is not allowed, otherwise it is set to a small factor (δ). This small value depicts the inconvenience caused by load shifting even if the shifting is allowed. This penalty assures that only shiftable loads are shifted from customers willing to participate in the DR program. Finally, the adjusted load (P^{ladj}_t) after DR can be computed using the original load (P^{lo}_t) and amount of load shifted to/from that interval, as given by (25). This adjusted load will be used in the power balancing equation in the islanded mode.

$$\sum_{t' \in T} P^{ls}_{t',t} \leq \left\{ \begin{matrix} 0 & if\ P^{nl}_t > 0 \\ TO^{\max}_t & else \end{matrix} \right\} \quad (22)$$

$$\sum_{t' \in T} P^{ls}_{t,t'} \leq FR^{\max}_t = P^{Shift}_t \quad (23)$$

$$v_{t,t'} = \left\{ \begin{matrix} \delta & if\ shifting\ is\ allowed \\ \infty & else \end{matrix} \right\} \quad (24)$$

$$P^{ladj}_t = P^{lo}_t + \sum_{t' \in T} P^{lsf}_{t',t} - \sum_{t' \in T} P^{ls}_{t,t'} \quad \forall t \neq t' \quad (25)$$

C. SOLUTION METHOD

The grid-connected operation mode is a preparation phase for an upcoming event. Therefore, robust- optimization is adopted to prepare for the worst-case scenario. However, the islanded mode is the testing phase of the resilience algorithm and various scenarios could occur in the real life. Therefore, in islanded mode, several scenarios are generated to test the performance of the proposed algorithm. The subscript s in the uncertain parameters of the islanded mode model represents scenario s, where $s \in S$. The uncertainties are randomly generated for each scenario within the decided dynamic bounds for each interval of time.

D. PROPOSED RESILIENCE INDEX

Various indices for evaluating the vulnerability and resilience of power systems are available in the literature. Panteli *et al.* [24], [35] have proposed a resilience achievement worth index for different corridors of transmission systems. These indices can be utilized to access the vulnerability of the system. Various indices have been proposed by [12] for assessing the resilience of the microgrids. However, the focus of these indices is to evaluate the outage of lines and recovery of the grid. Gao *et al.* [6] and Luo *et al.* [36] have proposed a resilience index to evaluate the resilience of microgrids as a function of survived critical loads only. However, survivability of non-critical loads also contributes to the resilience of the system. Therefore, a resilience index is proposed in this study considering survivability of all the loads with different priorities in the system.

The proposed resilience index is realized by using Equations (26)-(28). The resilience index at each time interval (RI_t) can be computed using the actual amount of load on AC side (P^{al}_{t,ρ_n}), DC side (P^{dl}_{t,ρ_n}), and the amount of load recovered from AC side ($P^{al}_{t,\rho_n,r}$) and DC side ($P^{dl}_{t,\rho_n,r}$) microgrids (26). Where, ρ_n represents the priority of n$^{\text{th}}$ level, i.e. $\rho_1 > \rho_2 > ...\rho_N$. Similarly, Nrepresents the maximum number of load levels in the microgrid. Equation (27) gives the maximum value of the resilience index ($RI_{\max}$) and the possible range of the resilience index. The normalized values of the resilience index ($\bar{RI}_t$) and acceptable range of the proposed resilience index (RI_{acc}) can be computed using (28).

The proposed resilience index is utilized to evaluate the performance of a given system against any major disruption event. The optimization results obtained from the conventional operation schemes and the proposed resilient operation strategy are evaluated using the proposed resilience index. The values of the proposed index vary between zero and one. Zero indicates the least resilient system and one indicates the most resilient systems. An acceptable bound is defined for the proposed index using information of various load categories in the system. Equation (28) implies that at least the most critical loads should be survived to assure the value of the resilience index within acceptable bounds.

$$RI_t = \left(\sum_{n\in N} \rho_n.\left(P^{al}_{t,\rho_n,r}+P^{dl}_{t,\rho_n,r}\right)\Big/\left(P^{al}_{t,\rho_n}+P^{dl}_{t,\rho_n}\right)\right)\Big/N \quad \forall n,t \tag{26}$$

$$RI_{\max} = \sum_{n\in N}\rho_n \Big/ N, \quad RI_t \in [0, RI_{\max}]\ \forall n,t \tag{27}$$

$$\bar{RI}_t = RI_t/RI_{\max}, RI_{\text{acc}} \in \left[1/(N.RI_{\max}), 1\right] \quad \forall n,t \tag{28}$$

V. INPUT DATA AND NUMERICAL SIMULATIONS

The AC/DC hybrid microgrid system shown in Fig. 1 is tested for evaluating the performance of the proposed method. The AC-side microgrid contains two micro-turbines, BESS, wind turbine, and loads. Similarly, the DC-side microgrid contains two fuel cells, BESS, EVs, photovoltaic array, and loads. Both AC and DC microgrids contain critical and non-critical loads. The AC and DC microgrids are interconnected through an interlinking converter and the utility grid is connected to the AC-side only. The efficiency of the interlinking converter is taken as 98% with a capacity of 200kW. The parameters of CDGs on AC and DC microgrids used for simulations are shown in Table 1. Similarly, the parameters of energy storage elements of the network are shown in Table 2. In grid-connected mode, a scheduling horizon of 24-hours with a time step of 1 hour is considered. In the islanded mode, scheduling from event occurrence time (te) to the end of the scheduling horizon (T) is considered. The details of other input data are explained in the following section. The objective of normal mode operation is to reduce the cost [37], [38] while the objective of the islanded mode is to enhance the service reliability to consumers [39].

TABLE 1. Parameters of CDGs of the network.

Parameters	AC CDGs		DC CDGs	
	CDG1	CDG2	CDG1	CDG2
Generation cost (KRW/kWh)	64	62	58	60
Maximum power (kW)	70	80	65	65
Minimum power (kW)	0	0	0	0
Start-up cost (KRW)	100	100	500	500
Shutdown cost (KRW)	50	50	300	300

TABLE 2. Parameters of storage elements of the network.

Parameters	AC BESS	DC BESS	EV
Capacity (kWh)	100	140	60
Charging/Discharging efficiency (%)	96	96	95
Initial SOC (%)	30	30	20
Minimum SOC (%)	20	20	20
Maximum SOC (%)	80	80	80
Target SOC (%)	-	-	50

A. INPUT DATA

The load data utilized in this study correspond to the actual consumption of the Department of Electrical and Electronic Engineering at Imperial College London for the year 2014.[1] The maximum load of the building is 446 kW, while the minimum load is 16 kW. The PV and wind generation profiles have been extracted from the Renewables Ninja database for 2014 using Imperial College's latitude and longitude as well as the height of the building (assuming that the wind turbines are installed on the roof of the building) [40]. The market prices have been extracted from ELEXON's website [41], who is the responsible body for administering the balancing and settlement code (BSC) in Great Britain and accordingly procures the services required to implement it. For the year under investigation, the system sells and buy prices have been found to be within the range (-150£/ MWh, 1528£/MWh). Probability density functions (PDFs) have been

[1]The load data have been provided in kind by the estate management office for the needs of this study.

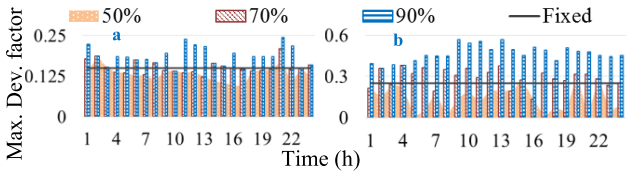

FIGURE 4. Max. deviation level on a working day: a) load; b) market price.

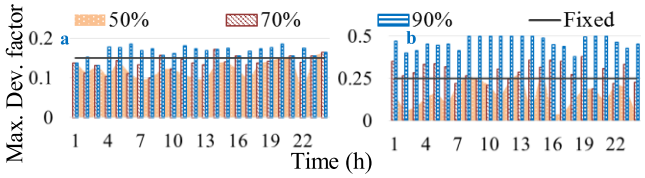

FIGURE 5. Max. deviation level on a holiday: a) load; b) market price.

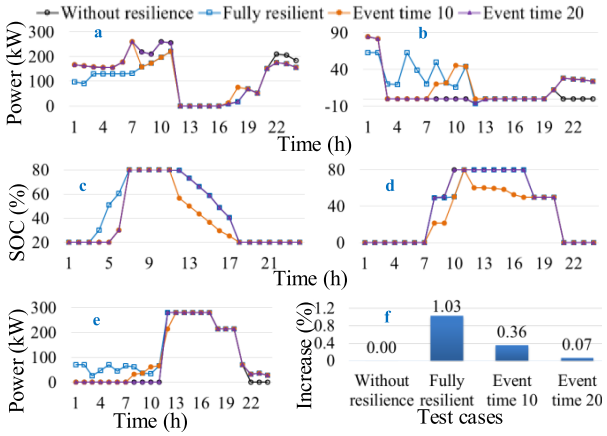

FIGURE 6. Operation results with different readiness levels: a) power trading with the utility grid; b) power transfer among AC and DC microgrids; c) SOC of BESS; d) SOC of EVs; e) power generation amount of CDGs; f) increase in operation cost.

constructed [42] utilizing these data and imported into Algorithm 1 for determining the lower and upper bounds.

B. NORMAL MODE OPERATION RESULTS

1) IMPACT OF MAXIMUM DEVIATION LEVEL

The objective of this section is to analyze the impact of the proposed dynamic bounds and the conventionally utilized static bounds. In order to determine the dynamic bounds, maximum deviation level is required. Therefore, maximum deviation levels for both the cases are analyzed in this section. The results of the proposed dynamic deviation bounds estimation algorithm along with conventional static bounds [14], [15], [17] are shown in Figs. 4 and 5. Fig. 4 shows the deviation bounds for load and market prices on a weekday (i.e. Monday) while Fig. 5 shows the bounds for a weekend day (i.e. Sunday). Due to the irrelevance of renewable energy amount on the day type, its results are not shown. However, the same method has been utilized to compute the maximum deviation bounds of renewables also. Various confidence interval levels (50%, 70%, and 90%) are considered for the proposed method. It can be observed from Figs. 4 and 5 that, the conventional bounds miscalculate (under- or overestimate) the impact of uncertain parameters. The differences in weekdays and weekends, dynamics across different times of the day and required confidence level are not reflected by the conventional static bounds. However, the proposed dynamic bounds, based on the historical data, can capture all these dynamics and mitigate the over-conservatism and/or infeasibility of the solution within the specified confidence interval level. The interval-wise fluctuations in the maximum deviation levels in Figs. 4 and 5 indicate that fixed bounds are not suitable for capturing uncertainty behavior of loads, renewables, and price signals.

2) IMPACT OF READINESS ON FEASIBLE ISLANDING

Readiness for a potential event can enhance the capability of the system to sustain events. In the meantime, conservative approaches can result in significant increase in the operation cost of the microgrid. Four cases are simulated in this section to evaluate the impact of readiness time on the operation of the microgrid. An 80% confidence interval has been selected for all prevailing uncertain parameters, i.e. loads, renewables, and market prices, in all the four cases. In the case without resilience-oriented operation, feasible islanding is not considered, and operation is only based on cost minimization (conventional operation). In the fully resilient case, irrespective of event occurrence time, feasible islanding is considered throughout the day. In the remaining two cases (event time 10 and event time 20), event preparation times start from 8 hours (8 h) and 18 hours (18 h), respectively based on the fragility curves. Preparation time for this system comes out as 2 hours ahead of the event occurrence time based on the pre-heat time/ramp rates of CDGs and C-rates of BESS and EVs in the tested microgrid system.

It can be observed from Fig. 6a that in the no-resilience case, electricity is bought from the utility grid during off-peak price intervals (1-11 h and 22-24 h) and CDGs are set to their minimum level (0 kW). However, in the fully resilient case, CDGs are not turned-off throughout the day to assure feasible islanding and correspondingly amount of power bought from the grid and transfer between AC and DC microgrids are reduced (Fig. 6b). Event time 10 case results follow without resilience case till 8 h and then follow the fully resilient case, due to activation of resilience at 8 h. It is the same case with event time 20 h with 18 h as the switching point. BESS has been fully charged during initial off-peak price hours and discharged during peak price hours, with slight variations for each case (Fig. 6c), in accordance with the resilience constraints. Similarly, usage of EV during its presence (8h to 20h) and achieving of target SOC (50%) before departure time (20h) can be observed from Fig. 6d. It can be observed from Fig. 6f that, operation cost has increased by 1.03% for the fully resilient case, considering without resilience case as the reference. However, the increase in cost turns out to be

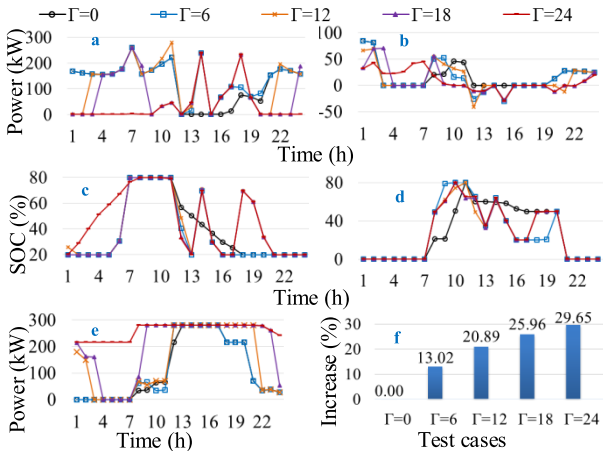

FIGURE 7. Operation results with different budget of uncertainty levels: a) power trading with the utility grid; b) power transfer among AC and DC microgrids; c) SOC of BESS; d) SOC of EV; e) power generation amount of CDGs; f) increase in operation cost.

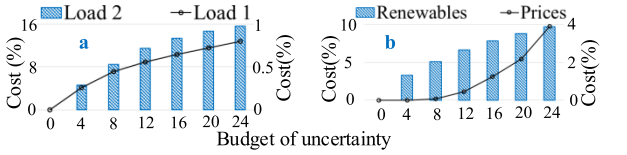

FIGURE 8. Uncertainty level in individual parameters and operation cost: a) non-critical (primary axis) and critical (secondary) loads; (b) renewables (primary axis) and market price (secondary axis).

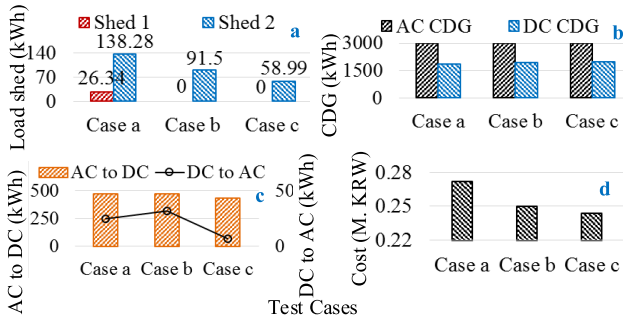

FIGURE 9. Day-1 operation results for all three cases: a) load shedding amount; b) CDG generated energy; c) energy transfer between AC and DC microgrids; d) operation cost.

0.36% and 0.07%, respectively for cases with event time 10 h and 20 h. It implies that information of event occurrence time can be utilized to control the increase in operation cost during the preparation phase.

3) IMPACT OF BUDGET OF UNCERTAINTY LEVEL

The budget of uncertainty decides the number of intervals during which a particular uncertain parameter can deviate from its forecasted values. Therefore, the budget of uncertainty is an important parameter to control the conservatism of the solution and to assure the feasibility of the solution. The impact of uncertainties on the operation of the microgrid is analyzed in this section. The event occurrence time is taken as 4 h (readiness preparation time from 2 h) for all the cases in this section. The values of the budget of uncertainty for all uncertain parameters are varied (0, 6, 12, 18, and 24), where $\Gamma = 0$ is the deterministic case and $\Gamma = 24$ is the worst-case. The budget of uncertainty can take a maximum value of 24 due to the presence of 24 intervals in the tested scheduling horizon.

Figs. 7a and 7e show that with an increase in Γ, the CDGs with lower generation cost is operated fully first, and then the remaining power shortage is fulfilled by buying power from the utility grid. Accordingly, power transfer between AC and DC microgrids is carried out to better utilize the cheaper CDG units on either sides, as shown in Fig. 7b. Fig. 7c and 7d show that with an increase in Γ, energy storage elements are more frequently charged/ discharged to cope with uncertainties. Finally, Fig. 7f shows that with an increase in Γ, the operation cost of the microgrid increases in a non-linear fashion. This is primarily due to the adjustment of power buying/selling from the grid by the operation algorithm. In addition, the presence of photovoltaic-based power during 12 hours (i.e. 7 am to 7 pm) of the day also contributes to this behavior.

Fig. 8 shows the impact of uncertainty in individual components on the operation cost of the microgrid. The increase in cost for non-critical loads (Load 2) is the highest due to the larger magnitude and a higher level of uncertainty. Similarly, the increase in cost for the critical loads (Load1) is the lowest due to the lower magnitude and lower uncertainty. Although the uncertainty in renewables is higher, the increase in cost for renewables is lower than the non-critical loads due to the lower magnitude, especially due to the presence of the photovoltaic power during half of the day only. The trend of market price is opposite to that of remaining three due to the ability to switch buying intervals with lower Γ values.

C. EMERGENCY MODE OPERATION RESULTS

In emergency mode operation, the operation of the current day and the following day are presented to analyze the impact of the proposed resilience-oriented operation method. During the first day operation, in conventional operation schemes, all the resources are utilized due to the absence of resilience-oriented DR programs. While in the following day even the critical loads may be shed due to the scarcity of the resources. The merits of the proposed survivability-oriented operation scheme, in this context, are presented in the following sections.

1) DAY-1 OPERATION RESULTS

The event occurrence time is taken as 4 a.m. and three cases are considered to evaluate the performance of the proposed resilience-oriented optimization algorithm including DR. In case a, both DR and resilience are not considered (conventional case) and in case b only resilience algorithm is considered. Finally, in case c both DR and resilience algorithm are considered.

Fig. 9a shows that load shedding was highest in case a and even some of the critical loads were also shed due to

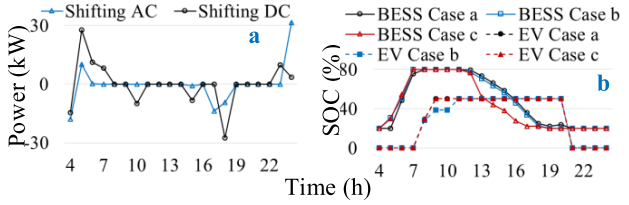

FIGURE 10. a) Load shifting in case c; b) SOC of energy storage elements.

unreadiness for the event. In case of b, none of the critical loads were shed and shedding of non-critical loads has reduced by 33.8% due to preparation for the event beforehand. In case c, load shedding of non-critical loads has reduced by 57.3% due to the incorporation of the DR program. The amount of AC CDG energy used is the same for all the cases, but DC CDG amount has increased from the case a to c due to preparedness and DR, as shown in Fig. 9b. Fig. 9c shows that power transfer has reduced from the case a to c due to the ability of each microgrid to manage the local loads via readiness and DR program. Similarly, Fig. 9d shows that operation cost has reduced from a to c due to reduction in load shedding amount. Fig. 10a shows that during case c, load from higher load intervals is shifted to other intervals having a lower load for maximum utilization of CDGs. Finally, BESS and EV are efficiently used to reduce the load shedding amount.

2) DAY-2 OPERATION RESULTS

It is assumed that the event persisted till the second day and operation results of the proposed resilience-oriented algorithm without DR (first case) and with DR (second case) are presented in this section. In order to elaborate the impact of the proposed DR program, higher renewable amount after the event is considered.

Fig. 11a shows that available CDGs are better utilized in the second case due to the ability to shift non-critical loads. Similarly, load shedding is reduced by 50.1% in the second case in comparison with the first case. The power transfer between AC and DC microgrids has increased to minimize the curtailment of renewables by adjusting loads in the second case, Fig. 11b. Correspondingly, the operation cost has reduced in the second case due to reduced load shedding. The load shifting in the second day is controlled by renewable power amount and more loads are shifted towards intervals having higher renewables (2-5, 22-24), Fig. 12a. Finally, BESS and EV are utilized to reduce curtailment of renewables and load shedding by charging during high renewable intervals as shown in Fig. 12b.

3) MONTE CARLO SIMULATIONS AND UNCERTAINTY ANALYSIS

The performance of the proposed resilience-oriented algorithm is evaluated under various possible scenarios of uncertainties in this section. Ten thousand scenarios of load and renewables are generated using Monte Carlo simulations.

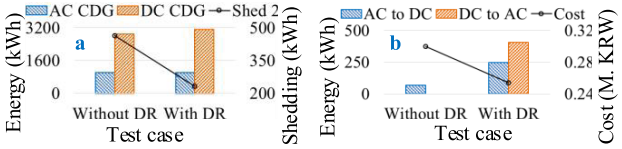

FIGURE 11. Day-2 operation results: a) CDG generated energy and load shedding amount; b) energy transfer between microgrids and operation cost.

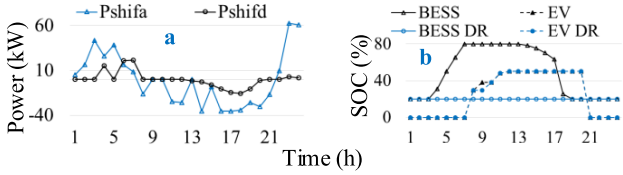

FIGURE 12. a) Load shifting in DR case; b) energy storage elements SOC.

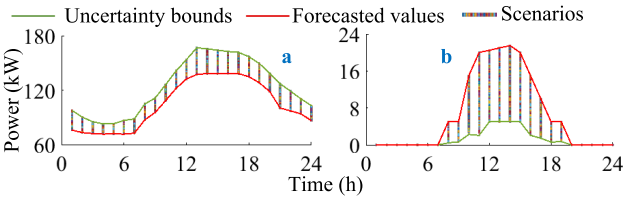

FIGURE 13. Simulation scenarios: a) load; b) renewable (PV).

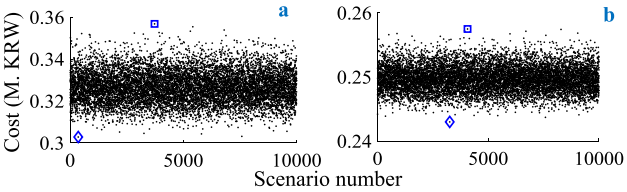

FIGURE 14. Operation cost: a) without resilience; b) with resilience.

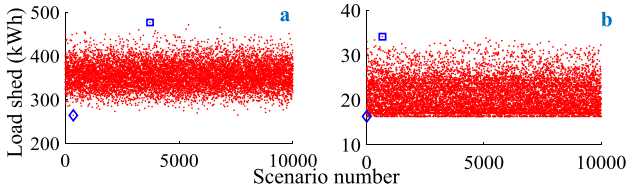

FIGURE 15. Load shedding amount: a) without resilience; b) with resilience.

Starting with hundred scenarios, the number of scenarios is increased by doubling the number until no further improvement is observed. It turns out to be ten thousand scenarios for this case. The bounds and generated scenarios for non-critical load of AC side and renewables of DC side are shown in Fig. 13. Scenarios for all other uncertain factors are also generated in the same way.

The impact of these scenarios on the operation cost, load shedding amount, and the proposed resilience index ($\bar{RI}_t$) are shown in Figs. 14-16, respectively. The results of the conventional operation case (without resilience) and the proposed

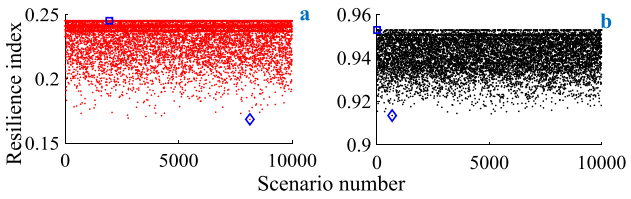

FIGURE 16. Resilience index value: a) without resilience; b) with resilience.

TABLE 3. Impact of resilient operation on operation cost.

Operation case	Without resilience	Event time (interval)			Fully resilient
		20	10	4	
Increase in cost (%)	0.00	0.07	0.36	0.92	1.03

TABLE 4. Impact of resilient operation on survivability.

Operation method	Resilient		Conventional	
Operation day	Day1	Day2	Day1	Day2
Load shedding (kWh)	58.99	231.66	164.62	464.07
Min. resilience index	0.94	0.95	0.24	0.72

resilience-oriented operation (with resilience) are presented in these figures. The square box represents the maximum value and the diamond box represents the minimum value. It can be observed from Fig. 14 that even the maximum operation cost value of the proposed method is lower than the minimum cost of the conventional method. This was due to the significant reduction of load shedding amount by the proposed method as shown in Fig. 15. It can be observed from Fig. 15 that load-shedding has been significantly reduced by the proposed resilience-oriented method via readiness and survivability. It can be observed from Fig. 16 that, the proposed method never violated the acceptable bound ([0.625, 1] according to (28)) while in case of the conventional method, the index value was always lower than the acceptable bound.

D. OPERATION COST AND SURVIVABILITY ANALYSIS

In this section, the performance of the proposed resilience-oriented operation scheme and conventional operation schemes (without resilience) are analyzed in terms of operation cost and survivability of the microgrid. It can be observed from Table 3 that the operation cost of the resilient scheme has increased in the preparation phase as compared to the without resilience case. The increase in the cost can be controlled by using the information of event as shown in Table 3. However, this increase in operation cost can reduce the amount of load shedding during event times due to readiness for islanding. In the case of conventional operation, a huge amount of load shedding is carried out at day1 (including the shedding of critical loads) and day2, as shown in Table 4. The proposed method had reduced the load shedding by about 4 times on the first day and by about 3 times on the second day as compared to the conventional method. The minimum value of the resilience index is below the acceptable bound for day1 in case of the conventional approach. However, none of the critical loads are shed in the proposed resilient scheme, i.e. resilience index is within the acceptable bound. It can be concluded from Tables 3 and 4 that, the resilient operation reduces load shedding significantly during emergencies with a minute increase in the operation cost during normal resilient operation.

VI. CONCLUSION

This paper has proposed an optimization strategy for enhancing the resilience of microgrids via readiness in the normal mode and survivability and demand response in the emergency mode. The increase in operation cost during readiness has been reduced using the fragility curves information to determine the preparation time. A data-driven approach is proposed to capture the dynamics of uncertain factors using historical data. Uncertainty in load has the highest impact on the operation cost due to a higher magnitude. In emergency mode, demand response has been utilized for enhancing service reliability of non-critical loads. Load shedding has been reduced by 57.3% and 50.1%, respectively for day-1 and day-2 operation with a minute increase in the operation cost during normal mode. Finally, Monte Carlo simulations have proved that the proposed method can assure the survivability of critical loads under various possible scenarios and enhance the service reliability to loads.

REFERENCES

[1] Y. Lin and Z. Bie, "Tri-level optimal hardening plan for a resilient distribution system considering reconfiguration and DG islanding," *Appl. Energy*, vol. 210, pp. 1266–1279, Jan. 2018.
[2] A. Gholami, T. Shekari, M. H. Amirioun, F. Aminifar, M. H. Amini, and A. Sargolzaei, "Toward a consensus on the definition and taxonomy of power system resilience," *IEEE Access*, vol. 8, pp. 32035–32053, 2018.
[3] L. Kleerekoper, M. Taleghani, A. den Dobbelsteen, and T. Hordijk, "Urban measures for hot weather conditions in a temperate climate condition: A review study," *Renew. Sustain. Energy Rev.*, vol. 75, pp. 515–533, Aug. 2017.
[4] S. Stanfield, J. Petta, and S. Baldwin, "Charging ahead: An energy storage guide for state policymakers," Interstate Renew. Energy Council, New York, NY, USA, Tech. Rep., 2017. Accessed: Jan. 17, 2019. [Online]. Available: https://irecusa.org/2017/04/irec-releases-energy-storage-guide-for-policymakers/
[5] T. Ding, Y. Lin, Z. Bie, and C. Chen, "A resilient microgrid formation strategy for load restoration considering master-slave distributed generators and topology reconfiguration," *Appl. Energy*, vol. 199, pp. 205–216, Aug. 2017.
[6] H. Gao, Y. Chen, Y. Xu, and C.-C. Liu, "Resilience-oriented critical load restoration using microgrids in distribution systems," *IEEE Trans. Smart Grid*, vol. 7, no. 6, pp. 2837–2848, Nov. 2016.
[7] Y. Xu, C.-C. Liu, K. P. Schneider, F. K. Tuffner, and D. T. Ton, "Microgrids for service restoration to critical load in a resilient distribution system," *IEEE Trans. Smart Grid*, vol. 9, no. 1, pp. 426–437, Jan. 2018.
[8] Z. Wang and J. Wang, "Self-healing resilient distribution systems based on sectionalization into microgrids," *IEEE Trans. Power Syst.*, vol. 30, no. 6, pp. 3139–3149, Nov. 2015.
[9] C. Chen, J. Wang, F. Qiu, and D. Zhao, "Resilient distribution system by microgrids formation after natural disasters," *IEEE Trans. Smart Grid*, vol. 7, no. 2, pp. 958–966, Mar. 2016.
[10] W. Yuan, J. Wang, F. Qiu, C. Chen, C. Kang, and B. Zeng, "Robust optimization-based resilient distribution network planning against natural disasters," *IEEE Trans. Smart Grid*, vol. 7, no. 6, pp. 2817–2826, Nov. 2016.
[11] T. Ding, Y. Lin, G. Li, and Z. Bie, "A new model for resilient distribution systems by microgrids formation," *IEEE Trans. Power Syst.*, vol. 32, no. 5, pp. 4145–4147, Sep. 2017.

[12] X. Liu, M. Shahidehpour, Z. Li, X. Liu, Y. Cao, and Z. Bie, "Microgrids for enhancing the power grid resilience in extreme conditions," *IEEE Trans. Smart Grid*, vol. 8, no. 2, pp. 589–597, Mar. 2017.
[13] K. P. Schneider, F. K. Tuffner, M. A. Elizondo, C.-C. Liu, Y. Xu, and D. Ton, "Evaluating the feasibility to use microgrids as a resiliency resource," *IEEE Trans. Smart Grid*, vol. 8, no. 2, pp. 687–696, Mar. 2017.
[14] M. H. Amirioun, F. Aminifar, and H. Lesani, "Towards proactive scheduling of microgrids against extreme floods," *IEEE Trans. Smart Grid*, vol. 9, no. 4, pp. 3900–3902, Jul. 2018.
[15] A. Gholami, T. Shekari, and S. Grijalva, "Proactive management of microgrids for resiliency enhancement: An adaptive robust approach," *IEEE Trans. Sustain. Energy*, vol. 10, no. 1, pp. 470–480, Jan. 2019.
[16] K. Balasubramaniam, P. Saraf, R. Hadidi, and E. B. Makram, "Energy management system for enhanced resiliency of microgrids during islanded operation," *Electr. Power Syst. Res.*, vol. 137, pp. 133–141, Aug. 2016.
[17] A. Hussain, V.-H. Bui, and H.-M. Kim, "A proactive and survivability-constrained operation strategy for enhancing resilience of microgrids using energy storage system," *IEEE Access*, vol. 9, pp. 75495–75507, 2018.
[18] A. Khodaei, "Resiliency-oriented microgrid optimal scheduling," *IEEE Trans. Smart Grid*, vol. 5, no. 4, pp. 1584–1591, Jul. 2014.
[19] A. Hussain, V.-H. Bui, and H.-M. Kim, "Optimal operation of hybrid microgrids for enhancing resiliency considering feasible islanding and survivability," *IET Renew. Power Gener.*, vol. 11, no. 6, pp. 846–857, May 2017.
[20] J. D. Lara, "Robust energy management systems for isolated microgrids under uncertainty," M.S. thesis, Dept. Elect. Comput. Eng., Univ. Waterloo, Waterloo, ON, Canada, 2014.
[21] R. Nateghi, "Multi-dimensional infrastructure resilience modeling: An application to hurricane-prone electric power distribution systems," *IEEE Access*, vol. 6, pp. 13478–13489, 2018.
[22] S. Dunn, S. Wilkinson, C. Galasso, L. Manning, and D. Alderson, "Development of empirical vulnerability curves for electrical supply systems subjected to wind hazard," in *Proc. ICASP*, Vancouver, BC, Canada, Jul. 2015, pp. 1–9.
[23] S. Dunn, S. Wilkinson, D. Alderson, and H. Fowler, "Fragility curves for assessing the resilience of electricity networks constructed from an extensive fault database," *Natural Hazards Rev.*, vol. 19, no. 1, p. 04017019, Feb. 2018.
[24] M. Panteli, C. Pickering, S. Wilkinson, R. Dawson, and P. Mancarella, "Power system resilience to extreme weather: Fragility modeling, probabilistic impact assessment, and adaptation measures," *IEEE Trans. Power Syst.*, vol. 32, no. 5, pp. 3747–3757, Sep. 2017.
[25] M. Jin, W. Feng, C. Marnay, and C. Spanos, "Microgrid to enable optimal distributed energy retail and end-user demand response," *Appl. Energy*, vol. 210, pp. 1321–1335, Jan. 2018.
[26] G. Carpinelli, F. Mottola, and D. Proto, "Optimal scheduling of a microgrid with demand response resources," *IET Generat., Transmiss. Distrib.*, vol. 8, no. 12, pp. 1891–1899, Apr. 2014.
[27] N. I. Nwulu and X. Xia, "Optimal dispatch for a microgrid incorporating renewables and demand response," *Renew. Energy*, vol. 101, pp. 16–28, Feb. 2017.
[28] C. Gouveia, J. Moreira, C. L. Moreira, and J. A. P. Lopes, "Coordinating storage and demand response for microgrid emergency operation," *IEEE Trans. Smart Grid*, vol. 4, no. 4, pp. 1898–1908, Dec. 2013.
[29] N. Rezaei and M. Kalantar, "Stochastic frequency-security constrained energy and reserve management of an inverter interfaced islanded microgrid considering demand response programs," *Int. J. Elect. Power Energy Syst.*, vol. 69, pp. 273–286, Jul. 2015.
[30] M. Bayat, K. Sheshyekani, M. Hamzeh, and A. Rezazadeh, "Coordination of distributed energy resources and demand response for voltage and frequency support of MV microgrids," *IEEE Trans. Power Syst.*, vol. 31, no. 2, pp. 1506–1516, Mar. 2016.
[31] A. Soroudi, P. Siano, and A. Keane, "Optimal DR and ESS scheduling for distribution losses payments minimization under electricity price uncertainty," *IEEE Trans. Smart Grid*, vol. 7, no. 1, pp. 261–272, Jan. 2016.
[32] A. Hussain, V.-H. Bui, and H.-M. Kim, "Robust optimal operation of AC/DC hybrid microgrids under market price uncertainties," *IEEE Access*, vol. 6, pp. 2654–2667, 2017.
[33] D. Bertsimas and V. Goyal, "On the power of robust solutions in two-stage stochastic and adaptive optimization problems," *Math. Oper. Res.*, vol. 35, no. 2, pp. 284–305, Mar. 2010.
[34] L. Zhao and B. Zeng, "Robust unit commitment problem with demand response and wind energy," in *Proc. IEEE Power Energy Soc. Gen. Meeting*, Jul. 2012, pp. 1–8.
[35] M. Panteli, D. N. Trakas, P. Mancarella, and N. D. Hatziargyriou, "Power systems resilience assessment: Hardening and smart operational enhancement strategies," *Proc. IEEE*, vol. 105, no. 7, pp. 1202–1213, Jul. 2017.
[36] D. Luo *et al.*, "Evaluation method of distribution network resilience focusing on critical loads," *IEEE Access*, vol. 6, pp. 61633–61639, 2018.
[37] Y. Chen, G. Xie, and R. Li, "Reducing energy consumption with cost budget using available budget preassignment in heterogeneous cloud computing systems," *IEEE Access*, vol. 6, pp. 20572–20583, 2018.
[38] J. Li, G. Xie, K. Li, and Z. Tang, "Enhanced parallel application scheduling algorithm with energy consumption constraint in heterogeneous distributed systems," *J. Circuits, Syst., Comput.*, to be published, doi: 10.1142/S0218126619501901.
[39] A. Hussain, V.-H. Bui, and H.-M. Kim, "A resilient and privacy-preserving energy management strategy for networked microgrids," *IEEE Trans. Smart Grid*, vol. 9, no. 3, pp. 2127–2139, May 2018.
[40] S. Pfenninger and I. Staffell, "Long-term patterns of European PV output using 30 years of validated hourly reanalysis and satellite data," *Energy*, vol. 114, pp. 1251–1265, Nov. 2016.
[41] ELEXON. (2018). *ELEXON Portal*. [Online]. Available: https://www.elexonportal.co.uk/news/latest?cachebust=2iuvrlbhge.
[42] H. Läuter and B. W. Silverman, *Density Estimation for Statistics and Data Analysis*. London, U.K.: Chapman & Hall, 1986.

AKHTAR HUSSAIN (S'14) received the B.E. degree in telecommunications from the National University of Sciences and Technology, Pakistan, in 2011, and the M.S. degree in electrical engineering from Myongji University, Yongin, South Korea, in 2014. He is currently pursuing the Ph.D. degree with Incheon National University, South Korea. His research interests include power system automation, smart grids, and microgrid operation.

ANASTASIOS OULIS ROUSIS (S'13) is currently pursuing the Ph.D. degree with Imperial College London. His research interests include the areas of power system optimization, renewables integration, the optimization of planning and operational models for transmission and distribution systems, while he investigates how flexible technologies can enhance the development of the future power systems.

IOANNIS KONSTANTELOS (M'12) received the M.Eng. degree in electrical and electronic engineering and the Ph.D. degree in electrical energy systems from Imperial College London, London, U.K., in 2007 and 2013, respectively. His research interests include mathematical programming and machine learning techniques applied to the planning and operation of energy systems.

GORAN STRBAC (M'95) is currently a Professor of energy systems with Imperial College London, London, U.K. His current research interests include the modeling and optimization of economics and the security of energy system operation and investment, energy infrastructure reliability, and future energy markets including the integration of emerging technologies in supporting cost-effective evolution to smart low carbon energy future.

JINHONG JEON (M'09) received the B.S. and M.S. degrees from Sungkyunkwan University, in 1995 and 1997, respectively, and the Ph.D. degree from the Department of Electrical Engineering, Pusan National University, South Korea, in 2012. Since 1997, he has been a Principal Researcher with the Smart Distribution Research Center, Korea Electrotechnology Research Institute, where he is currently a Technical Leader of the real-time simulation of distributed energy resource and microgrid. His research interests include different microgrids and its control aspects, including DC microgrids, hybrid microgrids, distributed energy resources, hierarchical and cooperative control, distributed control, and virtual synchronous machines.

HAK-MAN KIM (SM'15) received the first Ph.D. degree in electrical engineering from Sungkyunkwan University, South Korea, in 1998, and the second Ph.D. degree in information sciences from Tohoku University, Japan, in 2011. He was with the Korea Electrotechnology Research Institute, South Korea, from 1996 to 2008. He is currently a Professor with the Department of Electrical Engineering, Incheon National University, South Korea. His research interests include microgrid operation and control, and DC power systems.